SUPPLEMENTARY MATERIAL FOR:

The fate of fluvially-deposited organic carbon during transient floodplain storage

Scheingross, J.S.[1,2*], Repasch, M.N.[1,3], Hovius, N[1,3], Sachse, D.[1], Lupker, M.[4], Fuchs, M.[5], Halevy, I.[6], Gröcke, D.R.[7], Golombek, N.Y.[1,3,8], Haghipour, N.[4,9], Eglinton, T.I.[4], Orfeo, O[10], Schleicher, A.M.[1]

[1] GFZ-German Research Centre for Geosciences, Potsdam, Germany
[2] Department of Geological Sciences and Engineering, University of Nevada Reno, USA
[3] Institute of Geosciences, University of Potsdam, Germany
[4] Geological Institute, ETH Zürich, Zürich, Switzerland
[5] Helmholtz-Zentrum Dresden-Rossendorf, Helmholtz Institute Freiberg for Resource Technology, Germany
[6] Department of Earth and Planetary Sciences, Weizmann Institute of Science, Rehovot, Israel
[7] Department of Earth Sciences, Durham University, Durham, UK
[8] Department of Earth and Environmental Sciences, Dalhousie University, Halifax, Canada
[9] Laboratory of Ion Beam Physics, ETH Zürich, Zürich, Switzerland
[10] Centro de Ecología Aplicada del Litoral, CONICET, Corrientes, Argentina
*Corresponding author (jscheingross@unr.edu)

S1. Estimating the contribution from POC_{petro} in river and floodplain sediment

Oxidation of petrogenic organic carbon (POC_{petro}) and biospheric organic carbon (POC_{bio}) have different influences on the geologic carbon cycle (e.g., Hilton and West, 2020), and the presence of POC_{petro} can influence the isotopic signature of POC (e.g., Hilton et al., 2010), obscuring detection of isotopic changes caused by floodplain oxidation. While we do not use the relative proportions of POC_{petro} and POC_{bio} in Rio Bermejo sediment to estimate the potential for allochthonous POC oxidation in floodplain storage, our data does allow for estimating the presence of POC_{petro} in our samples. Given the interest in separating contributions of POC_{bio} and POC_{petro} to the geologic carbon cycle (e.g., Berner, 1999; Blair and Aller, 2012; Hilton and West, 2020; Horan et al., 2019), we provide such estimates in this supplement. These results do not influence the findings presented in the main text, except for the fact that our analyses suggest the presence of POC_{petro} in Rio Bermejo sediments, thereby making our estimates of oxidation of allochthonous POC in floodplain storage using Fm_{allo} (Section 4) a minimum bound on the total amount of oxidation of allochthonous POC in floodplain storage.

S1.1. Methods for isolating POC_{petro} contribution

We isolate POC_{petro} in floodplain and river sediment samples by solving for POC_{petro} weight percent (C_{org_petro}) using the *Galy et al.* (2008a) method, as well as a simple mixing model of *Fm* vs. 1/C_{org} (sensu Wang et al., 2019), which is free from autocorrelation present in the *Galy et al.* (2008a) method. Both the *Galy et al.* (2008a) method and simple mixing model method assume that C_{org_petro} is constant for all samples, such that variations in the total amount of POC and *Fm* among samples is due exclusively to variations in the POC_{bio} weight percent (C_{org_bio}). In some cases, we measured a total POC concentration less than the calculated POC_{petro} concentration, indicating the constant C_{org_petro} assumption was violated. For such cases, we set C_{org_petro} to its maximum possible value by assuming a binary mixture of POC_{bio} (assumed to have *Fm* = 1.07, the highest measured *Fm* in this study, Table S1) and POC_{petro} (*Fm* = 0) such that

$$C_{org\_petro} = C_{org}\left(1 - \frac{Fm}{1.07}\right) \quad \text{(S1)} .$$

Note that C_{org_petro} could exceed the value calculated in Eq. (S1) if samples contain POC biosynthesized after nuclear weapons testing when atmospheric *Fm* values exceeded 1.07.

Additionally, we independently estimated C_{org_petro} by attempting to remove POC_{bio} from a subset of samples with a H_2O_2 rinse prior to radiocarbon analysis. We leached ~5 g aliquots of select bedload and active bar deposits at room temperature in 10% H_2O_2 on a shaker table for >24 h prior to sample crushing and decarbonation (sensu Galy et al., 2008b). Following H_2O_2-leaching, samples had *Fm*>0 indicating incomplete removal of POC_{bio}. Assuming the leaching did not remove POC_{petro}, we estimated a maximum C_{org_petro} value for these samples following Eq. (S1) using C_{org} and *Fm* measured on the H_2O_2-leached aliquots.

S1.2. POC_{petro} content

C_{org_petro} for all river and floodplain samples overlapped within error, and we observed no systematic change in C_{org_petro} content between samples collected in the upstream versus downstream extent of the lowland Rio Bermejo (Figure S4). We estimated $0.03\% < C_{org\_petro} < 0.04\%$ and $0.007\% < C_{org\_petro} < 0.01\%$ using the method of *Galy et al.* (2008a) and the simple mixing model, respectively (Figure S4), which bound the range from the H_2O_2-rinsed samples ($0.007\% < C_{org\_petro} < 0.03\%$, Table S3). To estimate the fraction of POC_{petro} in the floodplain and river sediment samples, we followed Eq. (S1) to calculate a maximum C_{org_petro}. For samples in which C_{org_petro} calculated in Eq. (S1) was >0.04%, we reduced C_{org_petro} to 0.04% following the results of the *Galy et al.* (2008a) method, the simple mixing model, and the H_2O_2-rinsed samples. Using these estimates, the fraction of POC_{petro} contributing to the total POC in our samples (i.e., C_{org_petro}/C_{org}) ranged from 0.006–0.6 (Figure S4c); samples with lower C_{org} generally contained greater proportions of C_{org_petro} (Figure 5).

Figure Captions

Figure S1: Example photos of cored floodplain deposits, labeled by floodplain ID and minimum and maximum deposit ages (Table 1)

Figure S2: (a) R^2 values indicating the fit of linear regressions of the fractions of grains finer than a given value versus mineral specific surface area (SSA). (b) Fraction of grains finer than 2 µm (f_2) versus SSA.

Figure S3: Particulate organic carbon weight percent (C_{org}) (top row), stable carbon isotopic composition ($\delta^{13}C_{org}$) (middle row), and radiocarbon fraction modern (*Fm*) (bottom row) for actively-transported suspended and bedload sediment collected in the Rio Bermejo (a and c) and floodplain deposits (b and d) versus median particle size (D_{50}) (a and b) and Al/Si ratio (c and d). In panels (a and c), color and symbol groupings indicate distance downstream from the junction with the Rio San Francisco, while in panels (b and d) color and symbol show floodplain depositional age. Error bars show standard deviation from replicate measurements and are smaller than the symbol size where not shown.

Figure S4: Estimate of C_{org_petro} from suspended and bedload sediments following (a) *Galy et al.* (2008a) and (b) with a simple mixing model. Insets show enlarged version of the gray-shaded area in the main plot. C_{org} error bars denote standard deviation of multiple measurements, *Fm* error is analytical uncertainty, and error on the product C_{org} x *Fm* is propagated assuming random and uncorrelated error in C_{org} and *Fm* (Table S1). Error bars are smaller than the symbol where not shown. (c) Estimate of the fraction of petrogenic organic carbon to total organic carbon (C_{org_petro}/C_{org}) and (d) C_{org_petro} calculated following Eq. (S1) for samples with C_{org}<0.04%. In all panels, squares are floodplain sediment, circles are river sediment, and samples are split between upstream portions of the Rio Bermejo (<300 km straight-line distance from the Rio San Francisco junction) and downstream portions of the Rio Bermejo (>300 km straight-line distance from the Rio San Francisco junction).

Figure S5: Floodplain depth profiles of median grain size (D_{50}) and Al/Si ratio as a function of depth below the surface. (a and b) Show all profiles of D_{50} and Al/Si, respectively, on the same plot, color-coded by floodplain age. (c and d) Highlight individual profiles of D_{50} and Al/Si, respectively, for each floodplain core (black line) with profiles from other floodplain cores in gray. Plot axis extent of individual profiles in (c) and (d) match extent shown in (a) and (b), respectively. Error bars are removed for clarity, but are reported in Table S1. Box and whisker plots in (a) and (b) show median, inter-quartile range, and full extent of values observed in actively transported river sediments.

Figure S6: Comparison of POC weight percent (C_{org}) versus (a) Al/Si ratio and (b) median grain diameter (D_{50}) for actively transported river sediment (gray circles) and floodplain deposits (squares). Floodplains deposits are color-coded by depositional age and symbol size indicates sample depth below surface. Solid squares show measured C_{org}, and open squares show calculated allocthonous POC (C_{allo}) in floodplain samples. In cases where $C_{org} = C_{allo}$, only solid squares are shown. Error bars show standard deviation from replicate measurements, and are smaller than the symbol size when not shown. Floodplain deposit FP09 is ommitted from the figure as we have only a minimum a constraint (150 y) on its age.

Figure S7: Comparison of particle size distributions for the two oldest floodplain deposits (FP14 and FP15).

Tables (available as a single .xlsx file with tables in inidividual tabs)

Table S1: Particulate radiocarbon fraction modern (*Fm*), organic carbon weight percent (C_{org}), total nitrogen (TN) and stable carbon isotope values ($\delta^{13}C_{org}$) for river and floodplain sediment. Replicate columns of C_{org}, $\delta^{13}C$, and TN show measurements collected in individual runs. We use the mean and standard deviation of these measurements in all figures. River distance refers to the straight line distance downstream from the junction of the Rio San Francisco. Specific Surface Area measurements from Repasch et al. (2020).

Table S2: Optically stimulated luminesce and radiocarbon dating results for floodplain deposits (as reported in Repasch et al. (2020)). OSL analysis used quartz of 63 - 90 µm, 2 mm aliquots and the central age model (CAM (Galbraith et al., 1999)).

Table S3: Comparison of organic carbon weight percent (C_{org}) and stable carbon isotopes before and after rinsing samples in H_2O_2. We calculate maximum possible petrogenic organic carbon weight percent, C_{org_petro}, after H_2O_2 rinsing following Eq. (S1). River distance indicates the distance downstream from the junction with the Rio San Francisco junction. Samples with negative river distances are bedload from the Rio Bermejo and Rio San Francisco upstream of the junction of the two rivers. D_{50} indicates median grain size.

Supplemental References

Berner, R.A., 1999. A new look at the long-term carbon cycle. GSA Today 9.

Blair, N.E., Aller, R.C., 2012. The Fate of Terrestrial Organic Carbon in the Marine Environment. Annual Review of Marine Science, Vol 4 4, 401-423.

Galbraith, R.F., Roberts, R.G., Laslett, G.M., Yoshida, H., Olley, J.M., 1999. Optical dating of single and multiple grains of quartz from jinmium rock shelter, northern Australia, part 1, Experimental design and statistical models. Archaeometry 41, 339-364.

Galy, V., Beyssac, O., France-Lanord, C., Eglinton, T., 2008a. Recycling of Graphite During Himalayan Erosion: A Geological Stabilization of Carbon in the Crust. Science 322, 943-945.

Galy, V., France-Lanord, C., Lartiges, B., 2008b. Loading and fate of particulate organic carbon from the Himalaya to the Ganga-Brahmaputra delta. Geochimica Et Cosmochimica Acta 72, 1767-1787.

Hilton, R.G., Galy, A., Hovius, N., Horng, M.-J., Chen, H., 2010. The isotopic composition of particulate organic carbon in mountain rivers of Taiwan. Geochimica Et Cosmochimica Acta 74, 3164-3181.

Hilton, R.G., West, A.J., 2020. Mountains, erosion and the carbon cycle. Nature Reviews Earth and Environment 1, 284-299.

Horan, K., Hilton, R.G., Dellinger, M., Tipper, E., Galy, V., Calmels, D., Selby, J., Gaillardet, J., Ottley, C.J., Parsons, D.R., Burton, K.W., 2019. Carbon dioxide emissions by rock organic carbon oxidation and the net geochemical carbon budget of the Mackenzie River Basin. Am J Sci 319, 473-499.

Repasch, M., Wittmann, H., Scheingross, J.S., Sachse, D., Szupiany, R., Orfeo, O., Fuchs, M., Hovius, N., 2020. Sediment transit time and floodplain storage dynamics in alluvial rivers revealed by meteoric 10Be. J. Geophys. Res. Earth Surf.

Wang, J., Hilton, R.G., Jin, Z.D., Zhang, F., Densmore, A.L., Grocke, D.R., Xu, X.M., Li, G., West, A.J., 2019. The isotopic composition and fluxes of particulate organic carbon exported from the eastern margin of the Tibetan Plateau. Geochimica Et Cosmochimica Acta 252, 1-15.

Figure S1: Example photos of cored floodplain deposits, labeled by floodplain ID and minimum and maximum deposit ages (Table 1).

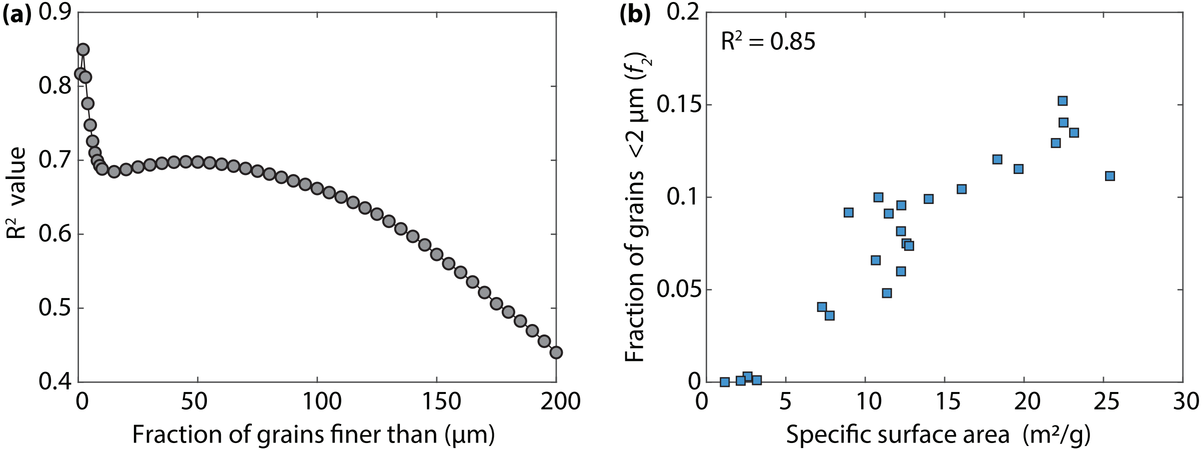

Figure S2: (a) R^2 values indicating the fit of linear regressions of the fractions of grains finer than a given value versus mineral specific surface area. (b) Fraction of grains finer than 2 μm (f_2) versus SSA.

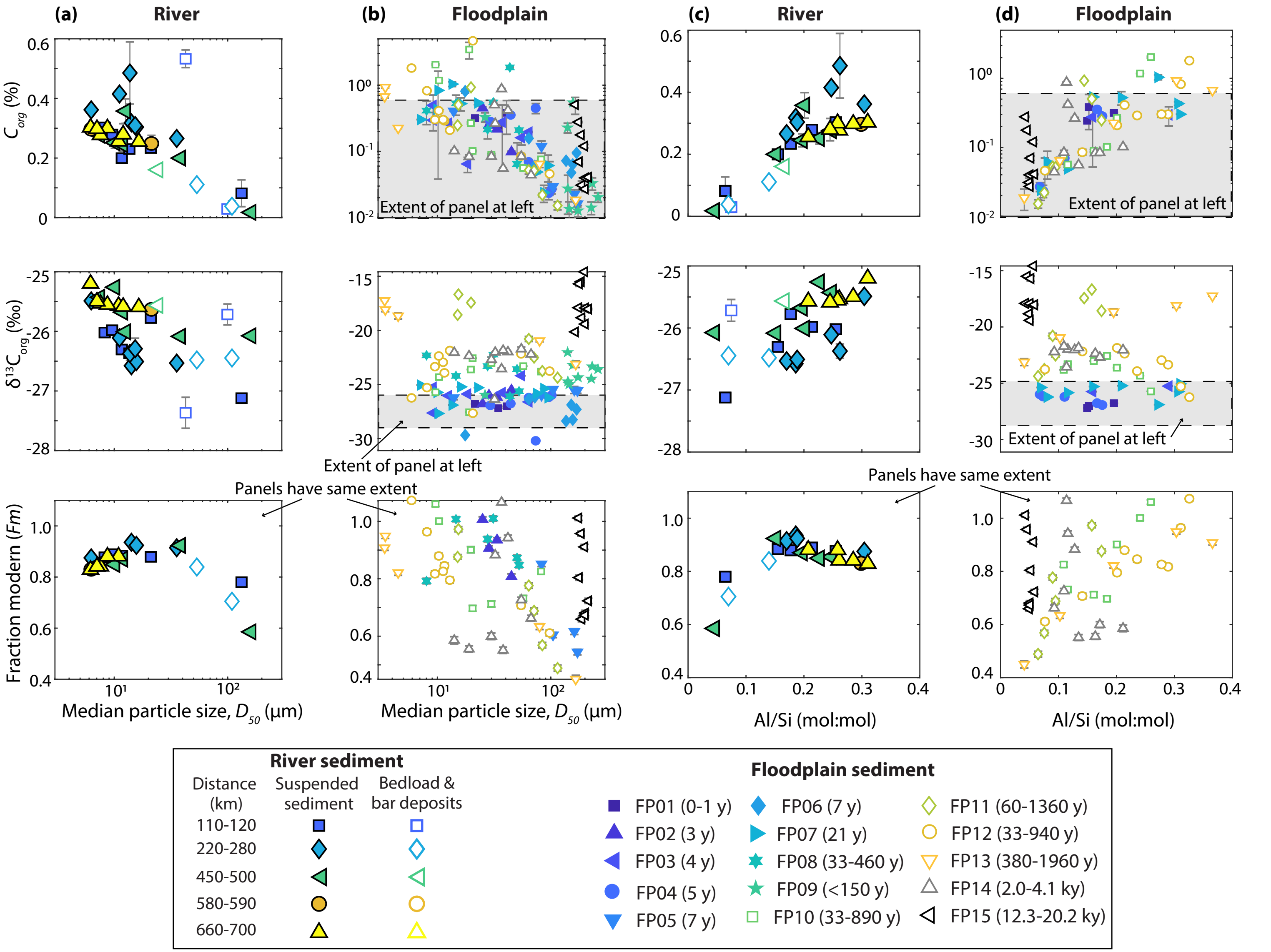

Figure S3: Particulate organic carbon weight percent (C_{org}) (top row), stable carbon isotopic composition ($\delta^{13}C_{org}$) (middle row), and radiocarbon fraction modern (*Fm*) (bottom row) for actively-transported suspended and bedload sediment collected in the Rio Bermejo (a and c) and floodplain deposits (b and d) versus median particle size (D_{50}) (a and b) and Al/Si ratio (c and d). In panels (a and c), color and symbol groupings indicate distance downstream from the junction with the Rio San Francisco, while in panels (b and d) color and symbol show floodplain depositional age. Error bars show standard deviation from replicate measurements and are smaller than the symbol size where not shown.

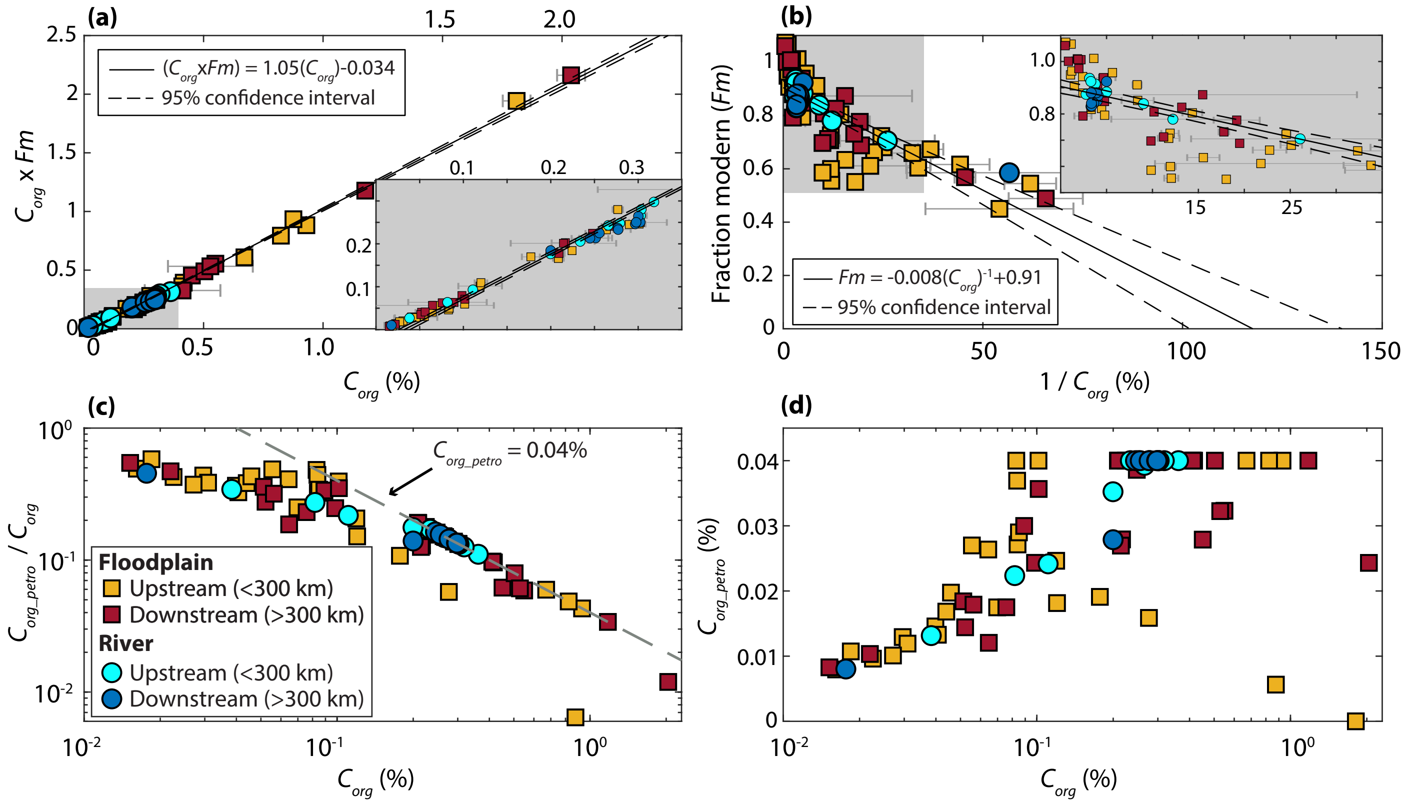

Figure S4: Estimate of C_{org_petro} from suspended and bedload sediments following (a) Galy et al. [2008a] and (b) with a simple mixing model. Insets show enlarged version of the gray-shaded area in the main plot. C_{org} error bars denote standard deviation of multiple measurements, *Fm* error is analytical uncertainty, and error on the product C_{org} x *Fm* is propagated assuming random and uncorrelated error in C_{org} and Fm (Table S1). Error bars are smaller than the symbol where not shown. (c) Estimate of the fraction of petrogenic organic carbon to total organic carbon (C_{org_petro}/C_{org}) and (d) C_{org_petro} calculated following Eq. (S1) for samples with C_{org}<0.04%. In all panels, squares are floodplain sediment, circles are river sediment, and samples are split between upstream portions of the Rio Bermejo (<300 km straight-line distance from the Rio San Francisco junction) and downstream portions of the Rio Bermejo (>300 km straight-line distance from the Rio San Francisco junction).

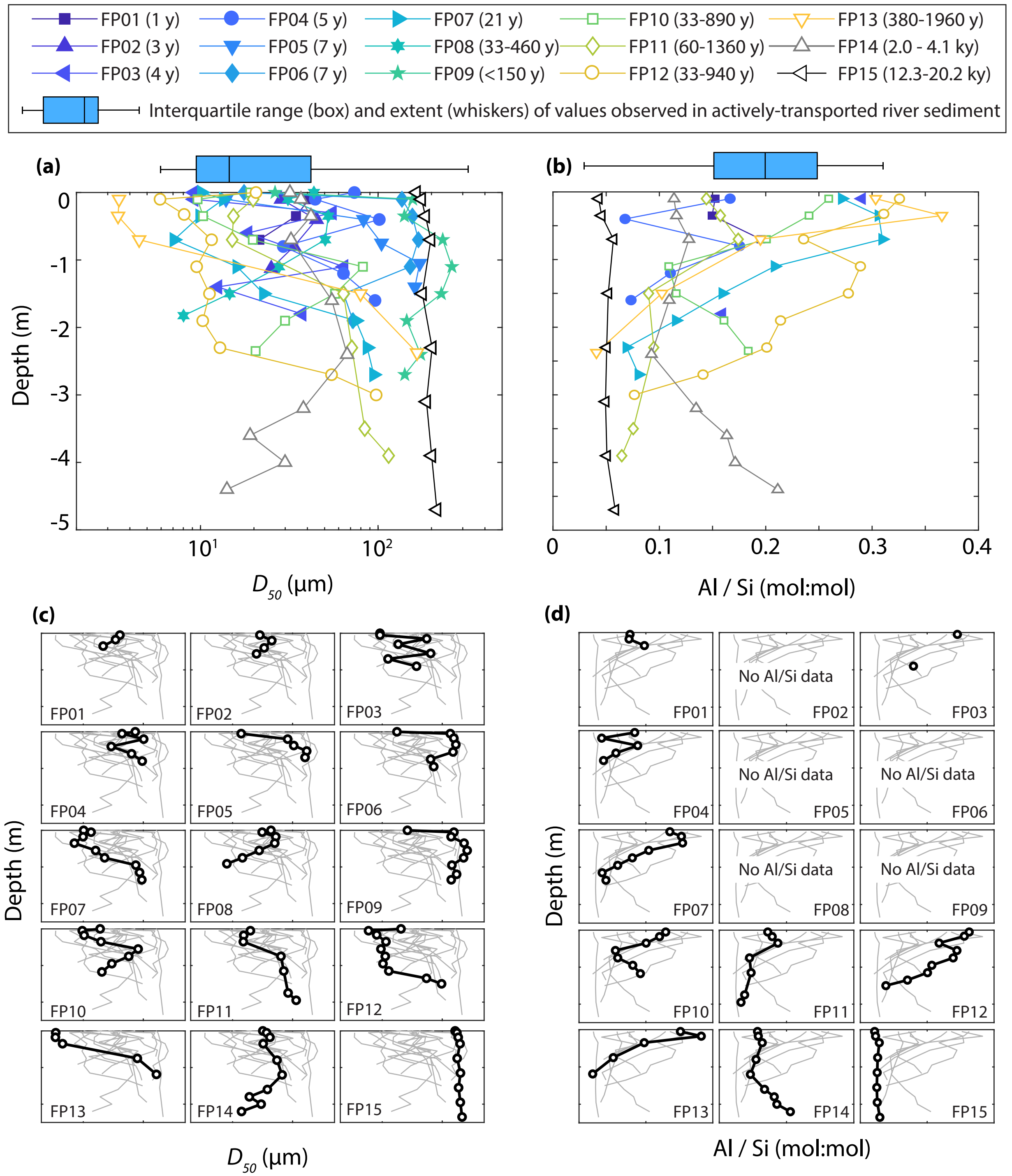

Figure S5: Floodplain depth profiles of median grain size (D_{50}) and Al/Si ratio as a function of depth below the surface. (a and b) Show all profiles of D_{50} and Al/Si, respectively, on the same plot, color-coded by floodplain age. (c and d) Highlight individual profiles of D_{50} and Al/Si, respectively, for each floodplain core (black line) with profiles from other floodplain cores in gray. Axis extent of individual profiles in (c) and (d) match extent shown in (a) and (b), respectively. Error bars are removed for clarity, but are reported in Table S1. Box and whisker plots in (a) and (b) show median, inter-quartile range, and full extent of values observed in actively transported river sediments.

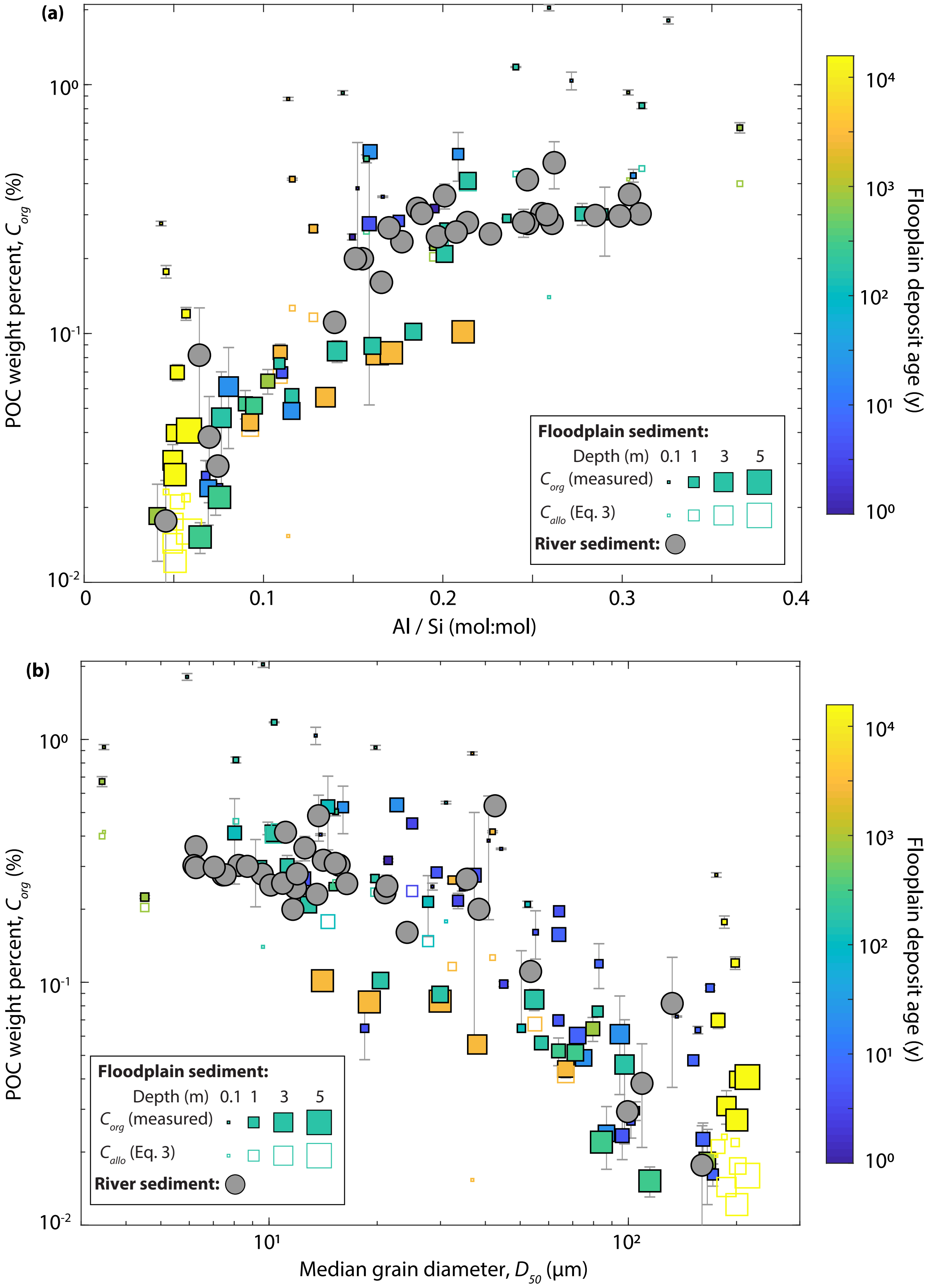

Figure S6: Comparison of POC weight percent (C_{org}) versus (a) Al/Si ratio and (b) median grain diameter (D_{50}) for actively transported river sediment (gray circles) and floodplain deposits (squares). Floodplains deposits are color-coded by depositional age and symbol size indicates sample depth below surface. Solid squares show measured C_{org}, and open squares show calculated allocthonous POC (C_{allo}). In cases where $C_{org} = C_{allo}$, only solid squares are shown. Error bars show standard deviation from replicate measurements, and are smaller than the symbol size when not shown. Floodplain deposit FP09 is ommitted from the figure as we have only a minimum a constraint (150 y) on its age.

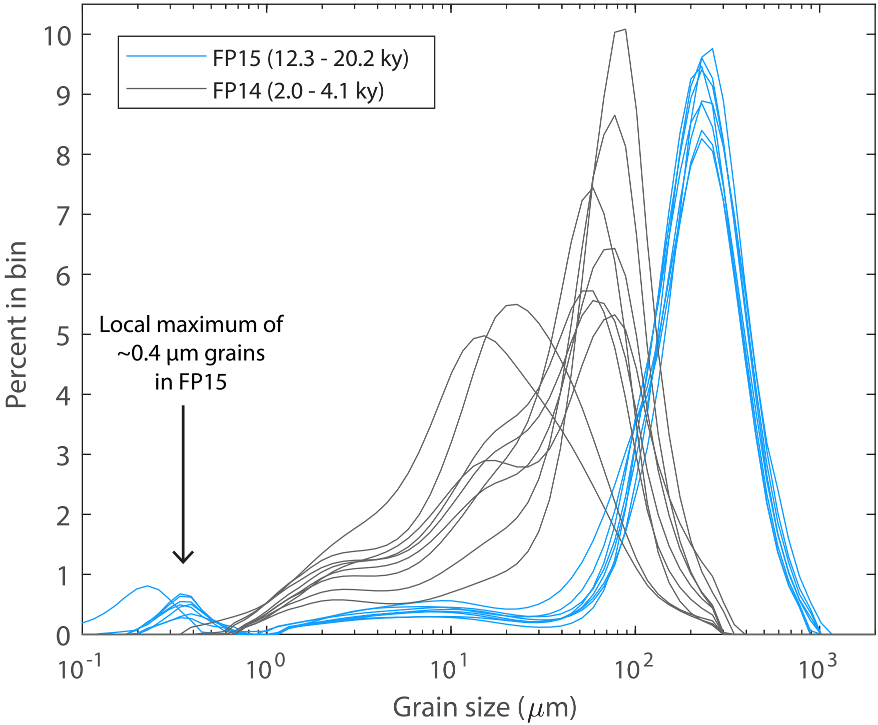

Figure S7: Comparison of particle size distributions for the two oldest floodplain deposits (FP14 and FP15).